materials

MDPI

Article

Compression Properties and Electrical Conductivity of In-Situ 20 vol.% Nano-Sized TiC_x/Cu Composites with Different Particle Size and Morphology

Dongdong Zhang [1], Fang Bai [1], Liping Sun [2], Yong Wang [1] and Jinguo Wang [1,*]

[1] Key Laboratory of Automobile Materials of Ministry of Education, Department of Materials Science and Engineering, Jilin University, Changchun 130025, China; ddzhang14@mails.jlu.edu.cn (D.Z.); baifang14@mails.jlu.edu.cn (F.B.); wyong15@mails.jlu.edu.cn (Y.W.)

[2] Cosco Logistics (Beijing) Materials Co., Ltd., No. 3 Maizidian West Road, Beijing 100016, China; hljsunlp@163.com

* Correspondence: jgwang@jlu.edu.cn; Tel./Fax: +86-431-8509-4699

Academic Editor: Yong-Cheng Lin
Received: 13 April 2017; Accepted: 2 May 2017; Published: 4 May 2017

Abstract: The compression properties and electrical conductivity of in-situ 20 vol.% nano-sized TiC_x/Cu composites fabricated via combustion synthesis and hot press in Cu-Ti-CNTs system at various particles size and morphology were investigated. Cubic-TiC_x/Cu composite had higher ultimate compression strength (σ_{UCS}), yield strength ($\sigma_{0.2}$), and electric conductivity, compared with those of spherical-TiC_x/Cu composite. The σ_{UCS}, $\sigma_{0.2}$, and electrical conductivity of cubic-TiC_x/Cu composite increased by 4.37%, 20.7%, and 17.8% compared with those of spherical-TiC_x/Cu composite (526 MPa, 183 MPa, and 55.6% International Annealed Copper Standard, IACS). Spherical-TiC_x/Cu composite with average particle size of ~94 nm exhibited higher ultimate compression strength, yield strength, and electrical conductivity compared with those of spherical-TiC_x/Cu composite with 46 nm in size. The σ_{UCS}, $\sigma_{0.2}$, and electrical conductivity of spherical-TiC_x/Cu composite with average size of ~94 nm in size increased by 17.8%, 33.9%, and 62.5% compared with those of spherical-TiC_x/Cu composite (417 MPa, 121 MPa, and 40.3% IACS) with particle size of 49 nm, respectively. Cubic-shaped TiC_x particles with sharp corners and edges led to stress/strain localization, which enhanced the compression strength of the composites. The agglomeration of spherical-TiC_x particles with small size led to the compression strength reduction of the composites.

Keywords: nano-sized TiC_x; size and morphology; compression properties; electrical conductivity

1. Introduction

Cu and Cu alloy have been used in electrical conductivities as functional materials because of their unique properties, such as high electrical and thermal conductivities [1,2], as well as good corrosion resistance in the atmosphere and seawater [3,4]. However, their low strength at high temperatures hampers their application. It is well known that TiC_x particles possess excellent properties, such as high melting point [5,6], high hardness [7,8], high Young's modulus [9], low density [10,11], low thermal expansion coefficient [12], and good chemical stability [13,14]. Therefore, adding TiC_x particles to Cu matrix makes it possible to possess both high thermal conductivity and electric conductivity in combination with high strength at the same time. Many studies have been conducted on the fabrication of in-situ TiC_x particles-reinforced Cu matrix composites [15–19]. For instance, Liang et al. [20,21] studied the in-situ mechanism of TiC_x in a Cu-Ti-C system and successfully prepared TiC_x-reinforced Cu matrix composites. Lu et al. [22] introduced 40–60 vol.% TiC-TiB_2 with an average particle size of 1.5 μm into molten Cu by in-situ method. They reported that the ultimate compression strength

increased by 123% for the composites compared with the unreinforced matrix. Liang et al. [23] investigated the thermal explosion reaction behavior of Cu-Ti-C systems with different Ti and C particle sizes, and the found that the sizes of C particles have a great influence on the ignition temperatures of the system. Wang et al. [24,25] used grounded carbon nanotubes (CNTs), which were treated via high speed ball milling, as carbon source to fabricate nano-sized TiC_x particle-reinforced Al matrix composites. Results showed that tensile strength was improved for the ball milling treatment of CNTs. Accordingly, a carbon source with small size is more needed in combustion synthesis.

It is well known that the mechanical properties and electrical conductivity of metal matrix composites are determined by size, morphology, and the distribution of the reinforced particles [26–29]. Yu et al. [30] proposed that the smaller size of primary Mg_2Si could improve the ultimate tensile strength of magnesium alloy. Wang et al. [31] fabricated various volume fraction TiC_x/Al composites with different particle sizes. They found that high volume fraction TiC_x/Al composites had higher compression strength, while where was no research concerning the effect of TiC_x size on the property of in-situ TiC_x/metal composites. Meijer et al. [32] studied the compression properties of the composites by finite element simulation, and they found that cubic particles could result in stress/strain localization in a unit cell model. However, almost no corresponding experiments were carried out to confirm the simulation results. As reported above, despite the fact that there are a few studies concerning the effect of particles content and sizes on the properties of particles-enhanced composites, the effects of different sizes and morphologies of particles on the properties of in-situ particles-reinforced metal matrix composites are very rare—especially Cu matrix composites.

In this research, 20 vol.% TiC_x/Cu composites with various particle sizes and morphologies were prepared by combustion synthesis combined with hot press consolidation in a Cu-Ti-CNTs system. Compression properties and electrical conductivity of the composites were investigated. These results provide an important guidance for the application of in-situ nano-sized TiC_x/Cu composites.

2. Experimental Procedure

The used raw materials were commercial powders of Cu (~45 μm), Ti (~25 μm), and CNTs (~10–25 nm in diameter and ~15–100 μm in length). Composites 1, 2, and 3 were fabricated by the method of combustion synthesis and hot press. The composites corresponding to mixing powders are shown in Table 1. The mixed powders in composite 1 consisted of raw CNTs, Ti, and Cu powders. Composite 2 contained ground CNTs, and raw Ti and Cu powders. The composition of powder in composite 3 was complicated, which included the pre-milled ground CNTs and Cu powders as well as raw Ti powder. The stoichiometric ratio of C/Ti was set to be 1:1. The nominal compositions of reactants were 80 vol.% Cu powders. In a cylindrical ceramic inwall container, ground CNTs was first prepared by milling at the speed of 300 r/min for 2 h, and then ground CNTs and Cu powders were pre-milled at the speed of 200 r/min for 8 h, the prepared mixed powders were finally separated and milled at the speed of 50 r/min for 24 h.

Table 1. Components of mixed powders for different composites. CNT: carbon nanotube.

Composites	Carbon Source	Pre-Milled	Mixed Powders
Composite 1	raw CNTs	–	raw CNTs + Cu + Ti
Composite 2	ground CNTs	–	ground CNTs + Cu + Ti
Composite 3	ground CNTs	ground CNTs + Cu	Pre-milled + Ti

After milling, the mixture powders were compressed into cylindrical compacts; the diameter of the compacts was 28 mm, the height was about 40 mm. Then, the cylindrical compacts were placed in a self-made vacuum furnace with hot press with high-purity argon gas (99.999%). When the temperature measured by W5-Re26 thermocouples rose rapidly, the composites were quickly pressed under the pressure of 40 MPa. Then, the vacuum furnace was cooled down via the water-cooling system to room temperature, and the composites were successfully fabricated.

The characterization of phase constitutions in the 20 vol.% TiC_x/Cu composites were carried out by X-ray diffraction (XRD, Rigaku D/Max 2500PC, Tokyo, Japan) with Cu Ka radiation at the scanning speed of 4°/min. The morphologies of the extracted TiC_x particles were examined by field emission scanning electron microscope (FESEM, JSM 6700, Tokyo, Japan) and high resolution transmission electron microscopy (HRTEM, JEM-2100F, Tokyo, Japan). The particle size in the size distribution images was measured one particle by one particle in 10 images by the software of nano-measure. The software gives the data and distribution of particle size. The microstructure of the composites was investigated by scanning electron microscopy (SEM, Evo18, Carl Zeiss, Oberkochen, Germany) with energy dispersive spectrometer (EDS) (Model Link-Isis, Oxford, UK). The mechanical properties were performed on a servo hydraulic materials testing system (MTS, MTS 810, Minneapolis, MN, USA) at a strain rate of 3×10^{-4} s^{-1}. The compression test was carried out three times every composite, and the middle curve was chosen as the final curve. The electrical conductivities of the TiC_x/Cu composites were measured through a digital eddy current metal conductivity meter (Sigma 2008b, Xiamen, China) at room temperature, the electrical conductivity results are quoted as % IACS (International Annealed Copper Standard).

3. Results and Discussion

Figure 1 shows the X-ray patterns of composites 1, 2, and 3. It can be found that TiC_x and Cu are detected and no obvious intermediate phases are observed, indicating that the 20 vol.% TiC_x/Cu composites were successfully fabricated via combustion synthesis in combination with hot press. Figure 2 shows SEM images and EDS analysis of etched surfaces of composites 1, 2, and 3. As indicated, the synthesized TiC_x particles homogeneously dispersed in the composites (Figure 2a–c). We conjecture that the use of CNTs with high specific surface results in the increase in the contact area between Cu-Ti liquid phase and CNTs, which promotes the in-situ reaction and thus leads to the uniform distribution of TiC_x in the composites. EDS analysis of the composites also shows that the various elements exhibit a uniform distribution, as shown in Figure 2d–i.

Figure 3a–c shows the FESEM images of the TiC_x particles extracted from composites 1, 2, and 3. The size distributions of TiC_x particles are shown in Figure 3d–f. As indicated in Figure 3a, most of the TiC_x particles in composite 1 are typically cubic in shape, with an average size of 96 nm. The TiC_x particles in composite 2 (Figure 3b) and composite 3 (Figure 3c) exhibit spherical and close-to-spherical shape with an average size of 94 nm and 49 nm, respectively. We believed that the decrease of particle size should be attributed to the high-speed pre-milling of Cu and CNTs powders. According to the viewpoint of Liang et al. [20], the mechanism of in-situ reaction is dissolution-precipitation in the Cu-Ti-C system. A small C source is conducive for [C] atoms to dissolve into Cu-Ti liquid phase to form Cu-Ti-C ternary liquid phase, reducing the heat for dissolution of [C] atoms compared with large C source, which would contribute to the decrease of TiC_x size.

Figure 4 shows the FESEM images of original Cu powder (Figure 4a,b) and mixed powders corresponding to composite 1 (Figure 4c,d). It can be seen that the large size distribution of CNTs on the surface of Cu powders is formed. Large CNTs are not conducive to the promotion of the dissolution of [C] atoms into Cu-Ti binary liquid phase, and thus lead to the increase in the concentration of local [C] atoms. Accordingly, the increase in the concentration of local [C] atoms results in high C/Ti mole ratio, which contributes to the formation of cubic-TiC_x. Figure 4e,f shows the mixed powders corresponding to composite 2. Shortened CNTs uniformly dispersed on the surface of Cu powder can be seen. For the pre-milled ones corresponding to composite 3 (Figure 4g,h), Cu powders were ground into small pieces during the high speed pre-milling process, and shortened CNTs uniformly distributed on the surface of copper powder, which increased the contact area between Cu and CNTs powders, in addition to promoting the in-situ reaction. Finally, the size of TiC_x particles decreased.

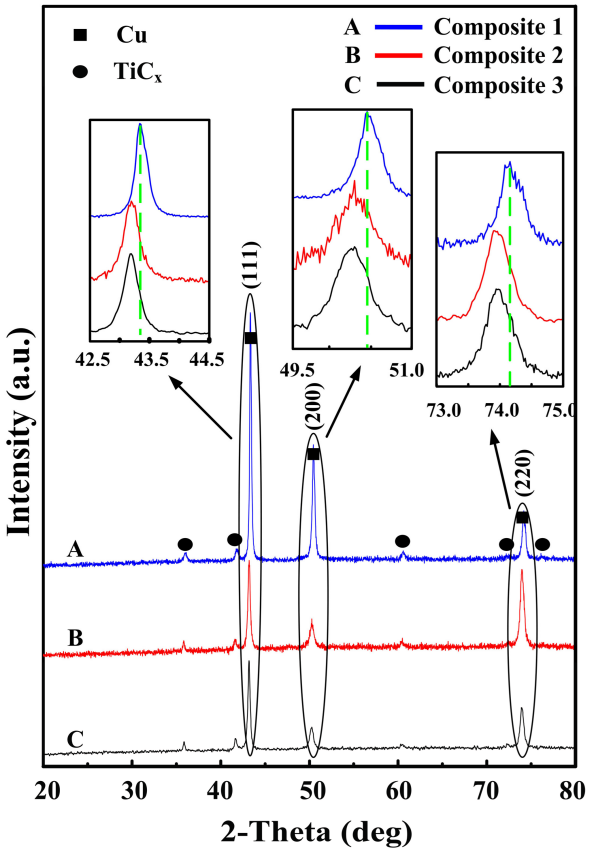

Figure 1. XRD patterns of composites 1, 2, and 3.

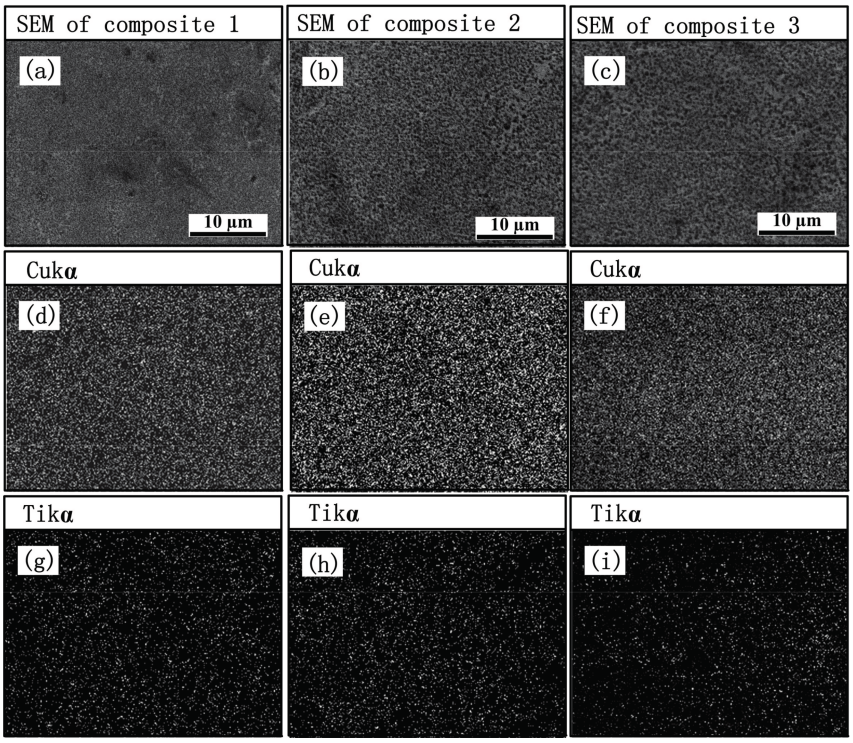

Figure 2. (**a**–**c**) SEM images and (**d**–**i**) energy dispersive spectrometry (EDS) of etched surfaces of composites 1, 2, and 3.

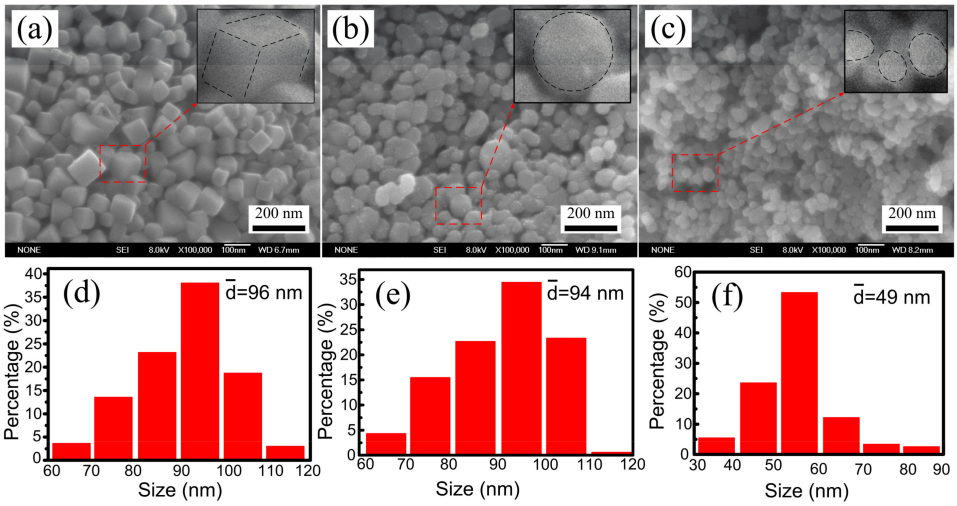

Figure 3. (**a**–**c**) Field emission SEM (FESEM) images and (**d**–**f**) corresponding size distribution of the TiC_x particles extracted from composites 1, 2, and 3.

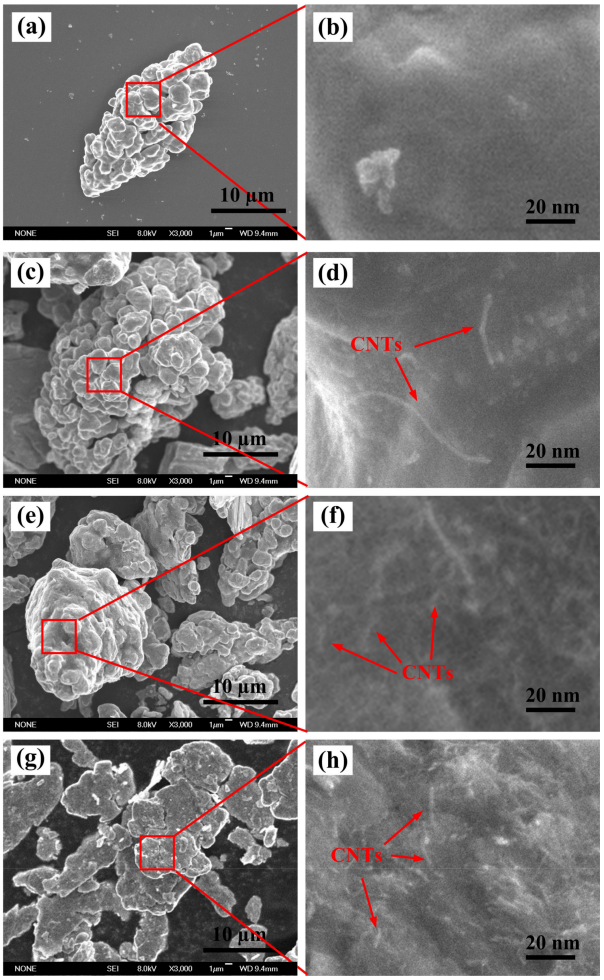

Figure 4. Morphologies of original Cu powders and mixed powders. (**a**) Original Cu powder; (**c**) mixed powders without pre-milling by using original CNTs as C source; (**e**) mixed powders pre-milled by using ground CNTs as C source; (**g**) mixed powders pre-milled by using ground CNTs as C source; (**b**,**d**,**f**,**h**) enlarged images corresponding to (**a**,**c**,**e**,**g**).

The compression engineering stress–strain curves of composites 1, 2, and 3 are shown in Figure 5. The compression properties data are listed in Table 2. As indicated, the yield strength ($\sigma_{0.2}$), ultimate compression strength (σ_{UCS}), and fracture strain (ε_f) of 20 vol.% TiC_x/Cu composites are improved with the increasing particles size. The σ_{UCS}, $\sigma_{0.2}$, and electrical conductivity of spherical-TiC_x/Cu composite (183 MPa, 526 MPa, and 55.6% IACS) with average size of ~94 nm increased by 17.8%, 33.9%, and 62.5% compared with those of spherical-TiC_x/Cu composite (417 MPa, 121 MPa, and 40.3% IACS) with particle size of 49 nm, respectively. The $\sigma_{0.2}$, σ_{UCS}, and electrical conductivity of 20 vol.% TiC_x/Cu composites were improved with the variation of particle shape from sphere to cube. The σ_{UCS}, $\sigma_{0.2}$, and electrical conductivity of cubic-TiC_x/Cu composite (549 MPa, 183 MPa, and 65.5% IACS) with particle size of 96 nm increased by 4.37%, 20.7%, and 17.8% compared with those of spherical-TiC_x/Cu composite (526 MPa, 183 MPa, and 55.6% IACS) with particle size of 94 nm. The fracture strains of composites 1, 2, and 3 are 25.9%, 35.7%, and 34.9%, respectively. Cubic-TiC_x/Cu composite with particle size of 96 nm had the highest $\sigma_{0.2}$, σ_{UCS}, and electrical conductivity among the three composites. Compared with the tensile strength (σ_b = 200~250 MPa) and yield strength ($\sigma_{0.2} \approx$ 60 MPa) of international annealed copper, the compression strength (σ_{UCS}) and yield strength ($\sigma_{0.2}$) of TiC_x/Cu composites were improved for the addition of particles with various particle sizes and shapes.

Table 2. Compression properties of the different composites.

Composites	$\sigma_{0.2}$/MPa	σ_{UCS}/MPa	ε_f/%
Composite 1	183^{+12}_{-14}	549^{+12}_{-15}	25.9^{+2}_{-3}
Composite 2	132^{+9}_{-13}	526^{+15}_{-13}	35.7^{+5}_{-3}
Composite 3	121^{+11}_{-14}	417^{+12}_{-15}	34.9^{+2}_{-2}

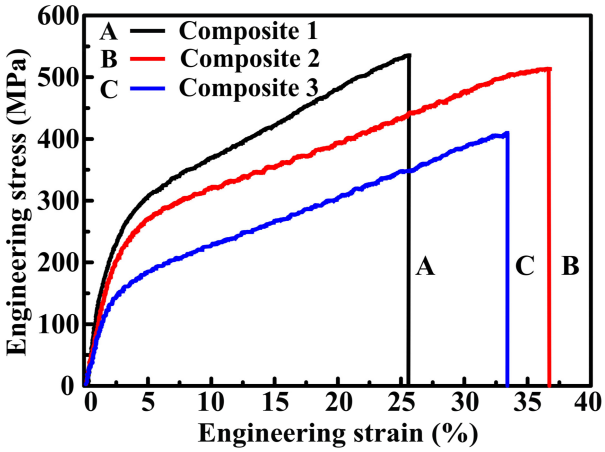

Figure 5. Compression engineering stress–strain curves of composites 1, 2, and 3.

Figure 6 shows TEM images of composite 1. The cubic-TiC_x particles are surrounded closely by Cu matrix, and there is a good interface between TiC_x particles and Cu matrix as shown in Figure 6a,b. The inset images of selected area electron diffraction pattern in Figure 6a corresponding to the [001] zone axis on cubic TiC_x particle also show a good interfacial bonding between the TiC_x particle and Cu matrix without cracks. According to the viewpoint of Meijer et al. [32], the cubic-shaped reinforced particles with sharp corners and edges lead to stress/strain localization. The elastic metal matrix provided constraint and produced high stress triaxiality for the particles. Accordingly, the initial strain hardening of composites reinforced by cubic-shaped particles is much higher than that of those reinforced by spherical-shaped particles. Following this viewpoint, it can be inferred that the σ_{UCS} and $\sigma_{0.2}$ of the composites with cubic-TiC_x particles can be greatly enhanced by the pinning effect and the stress concentration near edges and corners of cubic-TiC_x particles. As for the spherical TiC_x

particles, TiC_x particles with small size have higher surface energy and are easier to agglomerate than TiC_x particles with large size [24]. As a result, the agglomeration of TiC_x particles played a role as original crack, contributing to the performance reduction of the composite.

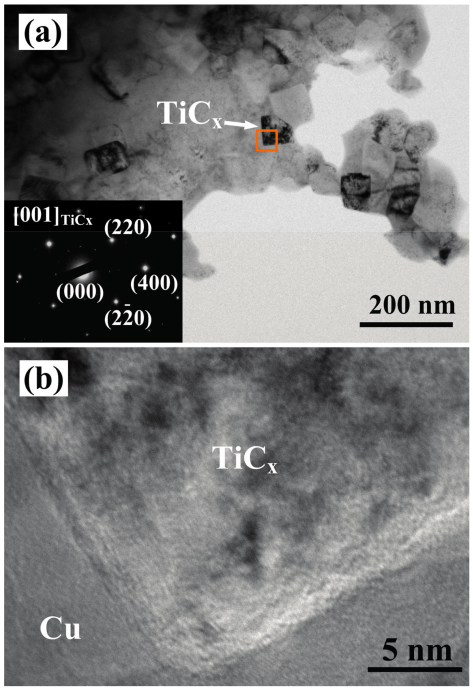

Figure 6. (**a**) TEM images of composite 1 and (**b**) enlarged image of the marked area of composite 1.

Figure 7 shows the electrical conductivities of composites 1, 2, and 3. As indicated, the electrical conductivities of the three composites are sensitive to the morphology and size of TiC_x particles, which are in the order of composite 1> composite 2 > composite 3. Composite 1, with cubic-TiC_x particles, had higher conductivity than that of composite 2, with spherical TiC_x particles. The electrical conductivity of composite 2, with large particle size, was higher than that of composite 3, with small particle size.

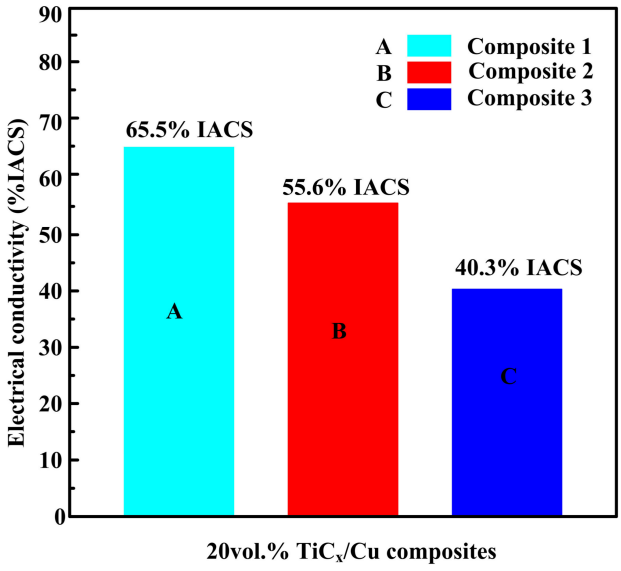

Figure 7. Electrical conductivities of composites 1, 2, and 3.

According to the viewpoint of Zhou [33] et al., the x value of TiC_x in substoichiometric analysis corresponding to cubic and spherical TiC_x were 0.875 and 0.625, which means that a part of Ti was residual except for the formation of TiC_x; besides, residual Ti is more in spherical-TiC_x/Cu composites than that in cubic-TiC_x/Cu composites on the basis of the substoichiometric analysis. According to Bragg's law ($\lambda = 2d\sin\theta$), the substitution of Ti for Cu leads to the expansion of the lattice (shift to low angle), since the atomic radius Ti is bigger than that of Cu atoms in Cu lattices, causing the diffraction peaks to shift to a lower angle. The more Ti solution, the lower the peaks will shift to. As described in the inset images of the corresponding area of the X-ray diffraction results in Figure 1, the peaks of Cu in composites 2 and 3 with lower angles mean that residual Ti atoms interact with Cu atoms to form the Cu solid solution; namely, provided more Ti atoms solute in the Cu matrix, the diffraction peak of Cu atoms will shift to lower angles, and the influence of electron scattering will be enhanced. Therefore, we can conjecture that the electrical conductivity of composite 1 (cubic, 96 nm) is higher than those of composite 2 (spherical, 94 nm) and 3 (spherical, 49 nm). As for the spherical-TiC_x/Cu composite, TiC_x particles with smaller size have larger specific surface area, which leads to a larger interface between the TiC_x particles and matrix. Therefore, the scattering of the electron for TiC_x/Cu composites with TiC_x particles of 49 nm was thus enhanced, and the electrical conductivity was finally reduced.

4. Conclusions

The compression properties and electrical conductivity of in-situ 20 vol.% nano-sized TiC_x/Cu composites fabricated via combustion synthesis and hot press at different particle size and morphology were investigated. The results show that the morphology and particle size have a pronounced effect on the compression properties and electrical conductivity. The cubic-TiCx composites had the highest σ_{UCS} and $\sigma_{0.2}$ among the three composites. Cubic-TiC_x particles with edges and corners in the composites pinned the movement of the dislocation and grain boundary; moreover, the stress concentration near the edges and corners of cubic-TiC_x particles reduced the elongation of composites, both of which led to the improvement of the σ_{UCS} and $\sigma_{0.2}$ with sacrificing the ε_f. The σ_{UCS}, $\sigma_{0.2}$, and electrical conductivity of spherical-TiC_x/Cu composites with particle size of 94 nm were higher than those of spherical-TiC_x/Cu composites with particle size of 49 nm. The performance reduction of the TiC_x/Cu composite with decreasing particle size was attributed to the agglomeration of TiC_x particles, which played a role as the source of crack, contributing to the reduction of performance. Meanwhile, the increase in the interface between particles and matrix enhanced the scattering of the electron and reduced the electrical conductivity of the composite. The solution of more Ti atoms in Cu matrix for spherical-TiC_x/Cu composites resulted in the enhancement of electron scattering and the decrease in electrical conductivity compared with the cubic one.

Acknowledgments: This work is supported by the National Natural Science Foundation of China (NNSFC, No. 51571101), and the Project 985-High Properties Materials of Jilin University.

Author Contributions: Dongdong Zhang and Jinguo Wang conceived and designed the experiments; Dongdong Zhang, Fang Bai, and Yong Wang performed the experiments; Dongdong Zhang, Liping Sun, and Jinguo Wang analyzed the data; Dongdong Zhang wrote the paper, Liping Sun polished the manuscript.

Conflicts of Interest: The authors declare no conflict of interest.

References

1. Qiu, F.; Chu, J.G.; Hu, W.; Lu, J.B.; Li, X.D.; Han, Y.; Jiang, Q.C. Study of effect of Zr addition on the microstructures and mechanical properties of (TiC_x–TiB_2)/Cu composites by combustion synthesis and hot press consolidation in the Cu–Ti–B_4C–Zr system. *Mater. Res. Bull.* **2015**, *70*, 167–172. [CrossRef]
2. Shojaeepour, F.; Abachi, P.; Purazrang, K.; Moghanian, A.H. Production and properties of Cu/Cr_2O_3 nano-composites. *Powder Technol.* **2012**, *222*, 80–84. [CrossRef]
3. Akhtar, F.; Askari, S.J.; Shah, K.A.; Du, X.L.; Guo, S.J. Microstructure, mechanical properties, electrical conductivity and wear behavior of high volume TiC reinforced Cu-matrix composites. *Mater. Charact.* **2009**, *60*, 327–366. [CrossRef]

4. Liu, Q.; He, X.B.; Ren, S.B.; Liu, T.T.; Kang, Q.P.; Qu, X.H. Fabrication and thermal conductivity of copper matrix composites reinforced with Mo_2C or TiC coated graphite fiber. *Mater. Res. Bull.* **2013**, *48*, 4811–4817. [CrossRef]
5. Rahaei, M.B.; Yazdanirad, R.; Kazemzadeh, A.; Ebadzadeh, T. Mechanochemical synthesis of nano TiC powder by mechanical milling of titanium and graphite powders. *Powder Technol.* **2012**, *217*, 369–376. [CrossRef]
6. Yang, Y.F.; Mu, D.K.; Jiang, Q.C. A simple route to fabricate TiC-TiB_2/Ni composite via thermal explosion reaction assisted with external pressure in air. *Mater. Chem. Phys.* **2014**, *143*, 480–485. [CrossRef]
7. Qiu, F.; Han, Y.; Cheng, A.; Lu, J.B.; Jiang, Q.C. Effect of Cr Content on the Compression Properties and Abrasive Wear Behavior of the High-Volume Fraction (TiC–TiB_2)/Cu Composites. *Acta Metall. Sin.* **2014**, *27*, 951–956. [CrossRef]
8. Acharya, S.; Debata, M.; Acharya, T.S.; Acharya, P.P.; Singh, S.K. Influence of nickel boride addition on sintering behaviour and mechanical properties of TiC-Ni based cermets. *J. Alloys Compd.* **2016**, *685*, 905–912. [CrossRef]
9. Klinger, L.; Gotman, I.; Horvitz, D. In-situ processing of TiB_2/TiC ceramic composites by thermal explosion under pressure: Experimental study and modeling. *Mater. Sci. Eng. A* **2001**, *302*, 92–99. [CrossRef]
10. Yang, Y.F.; Jiang, Q.C. Reaction behaviour, microstructure and mechanical properties of TiC–TiB_2/Ni composite fabricated by pressure assisted self-propagating high-temperature synthesis in air and vacuum. *Mater. Des.* **2013**, *49*, 123–129. [CrossRef]
11. Shu, S.L.; Yang, H.Y.; Tong, C.Z.; Qiu, F. Fabrication of TiC_x-TiB_2/Al Composites for Application as a Heat Sink. *Materials* **2016**, *9*, 642. [CrossRef]
12. Li, W.J.; Tu, R.; Goto, T. Preparation of directionally solidified TiB_2–TiC eutectic composites by a floating zone method. *Mater. Lett.* **2006**, *60*, 839–843. [CrossRef]
13. Lee, J.W.; Munir, Z.A.; Ohyanagi, M. Dense nanocrystalline TiB_2-TiC composites formed by field activation from high-energy ball milled reactants. *Mater. Sci. Eng. A* **2012**, *325*, 221–227. [CrossRef]
14. Aminikia, B. Investigation of the pre-milling effect on synthesis of nanocrystalline TiB_2–TiC composite prepared by SHS method. *Powder Technol.* **2012**, *232*, 78–86. [CrossRef]
15. Zhao, Q.; Liang, Y.H.; Zhang, Z.H.; Li, X.J.; Ren, L.Q. Study on the Impact Resistance of Bionic Layered Composite of TiC-TiB_2/Al from Al-Ti-B_4C System. *Materials* **2016**, *9*, 708. [CrossRef]
16. Popov, V.A.; Shelekhov, E.V.; Prosviryakov, A.S.; Presniakov, M.Y.; Senatulin, B.R.; Kotov, A.D.; Khomutov, M.G. Particulate metal matrix composites development on the basis of in situ synthesis of TiC reinforcing nanoparticles during mechanical alloying. *J. Alloys Compd.* **2017**, *707*, 365–370. [CrossRef]
17. Jin, S.B.; Shen, P.; Zou, B.L.; Jiang, Q.C. Morphology Evolution of TiC_x Grains during SHS in an Al-Ti-C System. *Cryst. Growth Des.* **2009**, *9*, 646–649. [CrossRef]
18. Yang, Y.F.; Wang, H.Y.; Wang, J.G.; Jiang, Q.C. TiB_2 and TiC stainless steel matrix composites Effect of C particle size on the mechanism of self-propagation high-temperature synthesis in the Ni–Ti–C system. *J. Alloys Compd.* **2011**, *509*, 7060–7065. [CrossRef]
19. Zhou, D.S.; Qiu, F.; Wang, H.Y.; Jiang, Q.C. Manufacture of Nano-Sized Particle-Reinforced Metal Matrix Composites: A Review. *Acta Metall. Sin. Engl. Lett.* **2014**, *27*, 798–805. [CrossRef]
20. Liang, Y.H.; Han, Z.W.; Li, X.J.; Zhang, Z.H.; Ren, L.Q. Study on the reaction mechanism of self-propagating high-temperature synthesis of TiC in the Cu–Ti–C system. *Mater. Chem. Phys.* **2012**, *137*, 200–206. [CrossRef]
21. Liang, Y.H.; Zhao, Q.; Zhang, Z.H.; Li, X.J.; Ren, L.Q. Effect of B_4C Particle Size on the Reaction Behavior of Self-Propagation High-Temperature Synthesis of TiC–TiB_2 Ceramic/Cu Composites from a Cu–Ti–B_4C System. *Int. J. Refract. Met. Hard Mater.* **2014**, *46*, 71–79. [CrossRef]
22. Lu, J.B.; Shu, S.L.; Qiu, F.; Wang, Y.W.; Jiang, Q.C. Compression properties and abrasive wear behavior of high volume fraction TiC_x–TiB_2/Cu composites fabricated by combustion synthesis and hot press consolidation. *Mater. Des.* **2012**, *40*, 157–162. [CrossRef]
23. Liang, Y.H.; Zhao, Q.; Li, X.J.; Zhang, Z.H.; Ren, L.Q. Effect of Ti and C particle size on reaction behavior of thermal explosion (TE) reaction of Cu-Ti-C system under Ar and air atmosphere. *J. Alloys Compd.* **2016**, *679*, 65–73. [CrossRef]
24. Wang, L.; Qiu, F.; Ouyang, L.C.; Wang, H.Y.; Zha, M.; Shu, S.L.; Zhao, Q.L.; Jiang, Q.C. A Novel Approach of Using Ground CNTs as the Carbon Source to Fabricate Uniformly Distributed Nano-Sized TiC_x/2009Al Composites. *Materials* **2015**, *8*, 8839–8849. [CrossRef]

25. Wang, L.; Qiu, F.; Zhao, Q.L.; Wang, H.Y.; Yang, D.L.; Jiang, Q.C. Simultaneously increasing the elevated-temperature tensile strength and plasticity of in situ nano-sized TiC_x/Al-Cu-Mg composites. *Mater. Charact.* **2017**, *125*, 7–12. [CrossRef]
26. Kampe, S.L.; Christodoulou, J.; Feng, C.R.; Christodoulou, L.; Michel, D.J. Effect of matrix microstructure and reinforcement shape on the creep deformation of near–γ titanium aluminide composites. *Acta Mater.* **1998**, *46*, 2881–2894. [CrossRef]
27. Chen, C.R.; Qin, S.Y.; Li, S.X.; Li, S.X.; Wen, J.L. Finite element analysis about effects of particle morphology on mechanical response of composites. *Mater. Sci. Eng. A* **2000**, *278*, 96–105. [CrossRef]
28. Xuan, Q.Q.; Shu, S.L.; Qiu, F.; Jin, S.B.; Jiang, Q.C. Different strain-rate dependent compression properties and work-hardening capacities of 50 vol% TiC_x/Al and TiB_2/Al composites. *Mater. Sci. Eng. A* **2012**, *538*, 335–339. [CrossRef]
29. Nie, J.F.; Wang, F.; Li, Y.S.; Cao, T.; Liu, X.F.; Zhao, Y.H.; Zhu, Y.T. Microstructure Evolution and Mechanical Properties of Al-TiB_2/TiC In Situ Aluminum-Based Composites during Accumulative Roll Bonding (ARB) Process. *Materials* **2017**, *10*, 109. [CrossRef]
30. Yu, H.C.; Wang, H.Y.; Chen, L.; Zha, M.; Wang, C.; Li, C.; Jiang, Q.C. Spheroidization of primary Mg_2Si in Al-20Mg_2Si-4.5Cu alloy modified with Ca and Sb during T6 heat treatment process. *Mater. Sci. Eng. A* **2017**, *685*, 31–38. [CrossRef]
31. Wang, L.; Qiu, F.; Shu, S.L.; Zhao, Q.L.; Jiang, Q.C. Effects of different carbon sources on the compressive properties of in situ high-volume-fraction TiC_x/2009Al composites. *Powder Metall.* **2016**, *59*, 370–375. [CrossRef]
32. Meijer, G.; Ellyin, F.; Xia, Z. Aspects of residual thermal stress/strain in particle reinforced metal matrix composites. Compos. *Part B Eng.* **2000**, *31*, 29–37. [CrossRef]
33. Zhou, D.S.; Jin, S.B.; Li, Y.J.; Qiu, F.; Deng, F.; Wang, J.G.; Jiang, Q.C. Effect of stoichiometry on the surface energies of {100} and {111} and the crystal shape of TiC_x and TiN_x. *CrystEngComm* **2013**, *15*, 643–649. [CrossRef]